Supplementary Information for

Single-Quantum Sodium MRI at 3T for the Separation of Mono- and Bi-T_2 Sodium Signals

Yongxian Qian,[1,2,*] Ying-Chia Lin,[1] Xingye Chen,[1,3] Yulin Ge,[1] Yvonne W. Lui,[1,4] Fernando E. Boada[1,†]

[1] Bernard and Irene Schwartz Center for Biomedical Imaging, Department of Radiology, New York University Grossman School of Medicine, New York, NY 10016.

[2] Neuroscience Institute, New York University Grossman School of Medicine, New York, NY 10016.

[3] Vilcek Institute of Graduate Biomedical Sciences, NYU Grossman School of Medicine, New York, NY 10016.

[4] Department of Radiology, NYU Langone Health, New York, NY 10016.

† Present address: Department of Radiology, Stanford University, Stanford, CA 94305.

* **Corresponding author**. Email: Yongxian.Qian@nyulangone.org

This PDF file includes:

Supplementary Text
Figs. S1 to S5
References (no)

Extrapolation of N-term exponential decay

We once accidently read a reference in literature about this topic, but could not find the citation at hand, thus summarize here the algorithm in our own language, specifically for the recovery of FID signals. If a signal $f(t)$ is an *N*-term exponential decay as defined in quation (S1) with parameters $\{A_i, b_i\ ;\ i = 1, 2, \ldots, N\}$, and is sampled at a uniform interval Δt, then a sample $f(t_0)$ at time t_0 can be represented by a linear combination of its late-time neighboring samples $\{f(t_0 + j\Delta t), j = 1, 2, \ldots, M\}$, as shown in equation (S2), with coefficients $\{a_j, j = 1, 2, \ldots, M \geq N\}$ to be determined.

$$f(t) = \sum_{i=1}^{N} A_i e^{-t \cdot b_i} \tag{S1}$$

$$f(t_0) = \sum_{j=1}^{M} a_j f(t_0 + j\Delta t) \tag{S2}$$

Proof. Extending $f(t_0 + j\Delta t)$ in equation (S2) according to equation (S1) gives

$$\begin{aligned} f(t_0) &= \sum_{j=1}^{M} a_j \left[\sum_{i=1}^{N} (A_i e^{-t_0 \cdot b_i})(e^{-j\Delta t \cdot b_i})\right] \\ &= \sum_{i=1}^{N} A_i e^{-t_0 \cdot b_i} \left(\sum_{j=1}^{M} a_j e^{-j\Delta t \cdot b_i}\right). \end{aligned} \tag{S3}$$

Select time-invariant coefficients $\{a_j, j = 1, 2, \ldots, M > N\}$ to satisfy equation (S4), thus equation (S2) holds.

$$\sum_{j=1}^{M} a_j e^{-j\Delta t \cdot b_i} = 1, \text{ for } i = 1, 2, \ldots, N. \tag{S4}$$

Note. The descriptions above are for backward extrapolation in time and used in the recovery of FID signal. The forward extrapolation also holds if Δt is replaced with $-\Delta t$ in equations (S2–S4). To find the unknown coefficients $\{a_j, j = 1,2, \ldots, M\}$, equation (S2), instead of equation (S4), is usually used on such a segment of $f(t)$ that it is not distorted and involves all the *N* exponential decays. The number of data samples on the segment should be larger than *M* to form an over-determined problem in case of random noise existing in the signal $f(t)$.

Correction for hardware-related distortion of FID signal

Fig. S1 demonstrates an FID signal from a healthy subject (52 years old, male), with and without correction for the distortion at the first five ADC samples using equation (S2) with (*M*, *N*) = (5, 3). The correction removed distortion and reduced overall residual fitting error from 2.33% to 1.49%. The correction also improved resolution of short-T_2* components: from singlet at 2.5ms to doublet at 0.5ms and 2.5ms (Figs. S1a3, b3).

Fig. S1. FID signal and T_2* spectrum with and without correction.

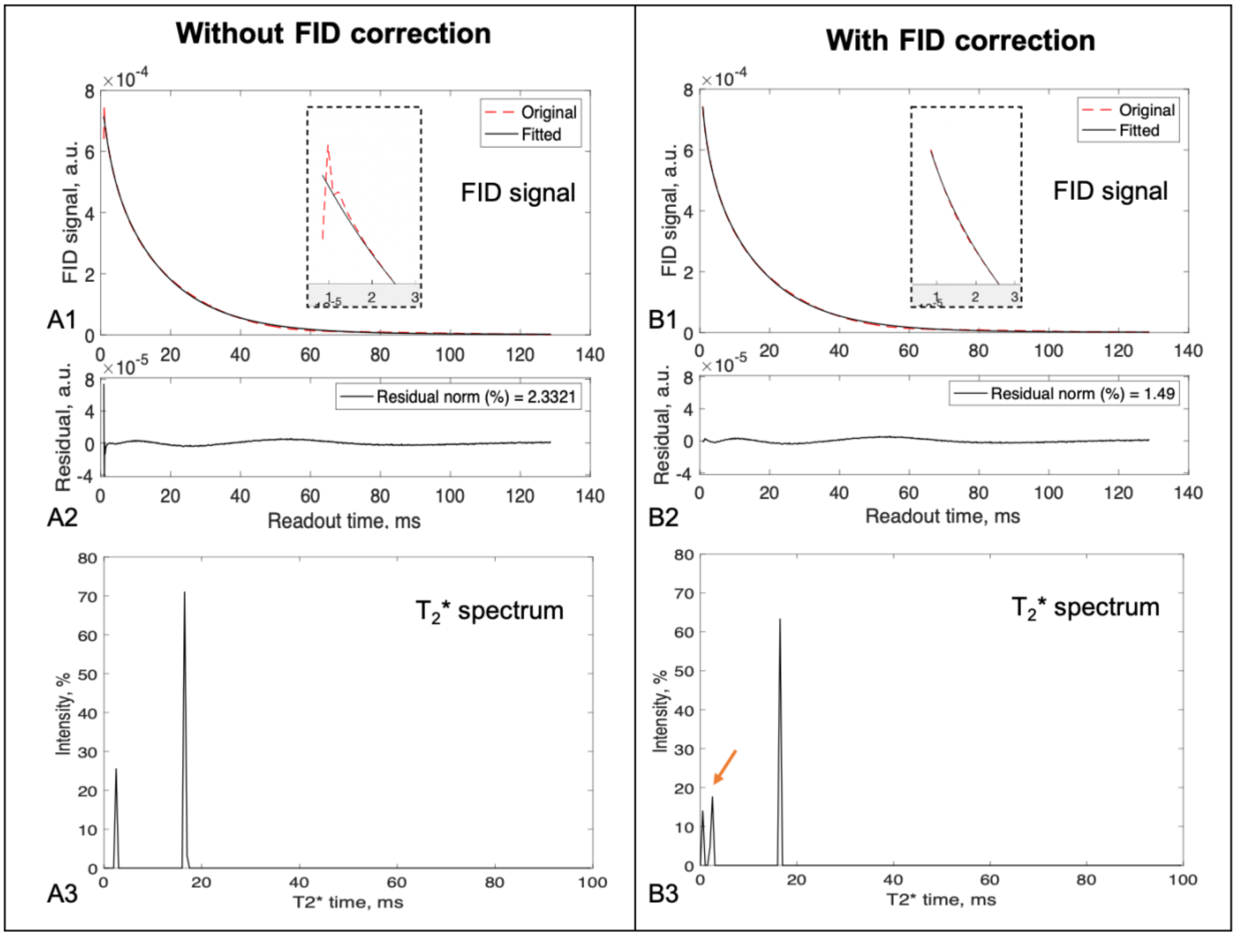

Fig. S1. FID signals (top) and T_2* spectra (bottom) from whole brain of a healthy subject (52 years old, male), with (Fig. S1b) and without (Fig. S1a) correction for FID distortion at the first five samples shown in the insets. In the middle are residual errors from the fitting using the T_2* spectra in the bottom. The FID correction removed the distortion, significantly reduced residual error, and clearly improved resolution of short-T_2* components from singlet at 2.5ms to doublet at 0.5ms and 2.5ms as well as peaks' intensity (Fig. S1b3). Data acquisition: 3T scanner (Prisma, Siemens) with a custom-built dual-tuned (^{1}H-^{23}Na) 8-channel head array coil [32], *fid* sequence, rectangular RF duration=0.5ms, TE/TR=0.35/300ms, averages=128, ADC samples=1024 at an interval of 0.125ms.

Calculation stability of T_2* spectrum at a high resolution of ΔT_2*=0.5ms

T_2* spectrum was calculated via equation (5) on an FID signal using an established algorithm – the non-negative least squares (NNLS) – at a high spectral resolution of ΔT_2*=0.5ms in a range of 0.5–100 ms. Such a high resolution raises a concern on the stability of calculation as the base functions at these spectral locations, $exp(-t/T_2^*)$, are not independent from each other. To address this concern, we employed singular value decomposition (SVD) to analyze the transfer matrix $\boldsymbol{E}$ in equations (S5) and used numerical simulations to detail the impact of random noise on the T_2* spectrum in equation (S6).

$$E_{i,j} \equiv exp\left(-t_i/T_{2,j}^*\right), \quad i = 1,2,\dots,N, \quad j = 1,2,\dots,M, \quad N \gg M \qquad \text{(S5a)}$$

$$\mathbf{E^T E} = \mathbf{U}\,\mathbf{\Sigma}\,\boldsymbol{V}^T \qquad \text{(S5b)}$$

$$\mathbf{\Sigma} = \text{diag}(\sigma_1, \sigma_2, \dots, \sigma_M) \qquad \text{(S5c)}$$

with sampling time $t_i = TE + (i-1) * \Delta t$ and spectral location $T_{2,j}^* = j * \Delta T_2^*$. Singular values $\left\{\sigma_j, j = 1,2,\dots,M\right\}$ determine stability of the calculation for T_2* spectrum in terms of random noise interference in equation (5). Correlation coefficients between the base functions are also calculated.

$$R_{j1,j2} = (E^T E)_{j1,j2} / \sqrt{(E^T E)_{j1,j1} (E^T E)_{j2,j2}}\,. \qquad j1, j2 = 1,2,\dots,M \qquad \text{(S6)}$$

At $\Delta t = 0.05$ms, *TE*=0.2ms and *N*=2048, the singular values and correlation coefficients were calculated and shown in Fig. S2. The singular value σ quickly decreases to zero ($<10^{-10}$) at index (15, 13, 10, 9) when ΔT_2* increases from 0.5ms to 1.0, 3.0 and 5.0 ms, respectively. This indicates the existence of null subspace or multiple solutions for T_2* spectrum (Fig. S2, top). The normalized correlation coefficients *R* between any two base functions is spreading out from diagonal line, confirming non-orthogonal between the base functions (Fig.S2, bottom). However, the extent of spreading is narrower for short T_2* values at high resolution ΔT_2* = 0.5ms than at low resolution ΔT_2* = 5ms.

Numerical simulations for the impact of random noise on the T_2* spectrum was performed at three popular components, T_2*=3, 15, and 50 ms with relative amplitudes A=30, 20, and 50, respectively, plus an additive normal random noise generated by function *randn(n,1)*, at SNR ≡ *f*(*t*=0)/SD = 100, 50, and 25. Outcomes of the simulations were summarized in Fig. S3, where peak parameters at doublets (Fig. S3, bottom) were linearly combined with amplitude-weighting by left- and right-peaklets in equation (S7). The best spectrum was achieved at SNR=100 among the three noisy cases, relative to no noise.

$$T_2^* = (A_L * T_{2,L}^* + A_R * T_{2,R}^*)/\text{A}, \qquad \text{(S7a)}$$

$$\text{A} = A_L + A_R \qquad \text{(S7b)}$$

Fig. S2. Calculation stability of T_2* spectrum.

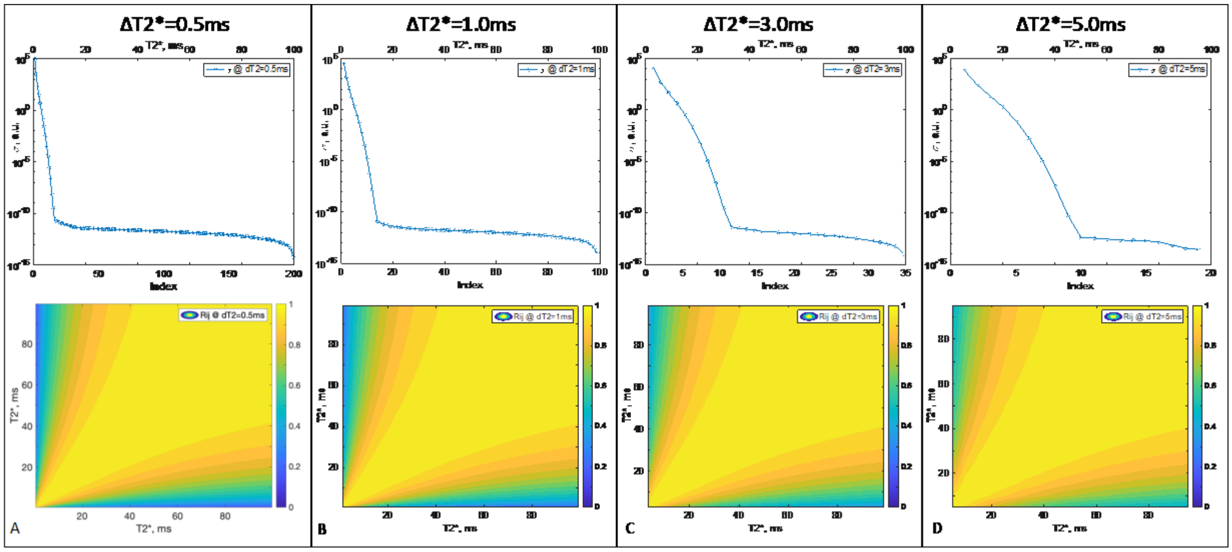

Fig. S2. The SVD singular values of matrix E^TE (top) and correlation coefficients of the base-in matrix E (bottom). **(A)** – **(D)** T_2* spectral resolution at $\Delta T_2* = 0.5, 1.0, 3.0$, and 5.0ms. In the top, singular value σ quickly decreases to zero ($<10^{-10}$) at index (15, 13, 10, 9) respectively, indicating the existence of null subspace or multiple solutions for the T_2* spectrum. In the bottom, the normalized correlation coefficient $R_{j1,j2}$ between any two T_2* base functions $\exp(-t/T_{2,j}*)$ is spreading out from diagonal line, showing non-orthogonal between the base functions.

Fig. S3. Numerical simulations for the impact of random noise on T_2* spectrum.

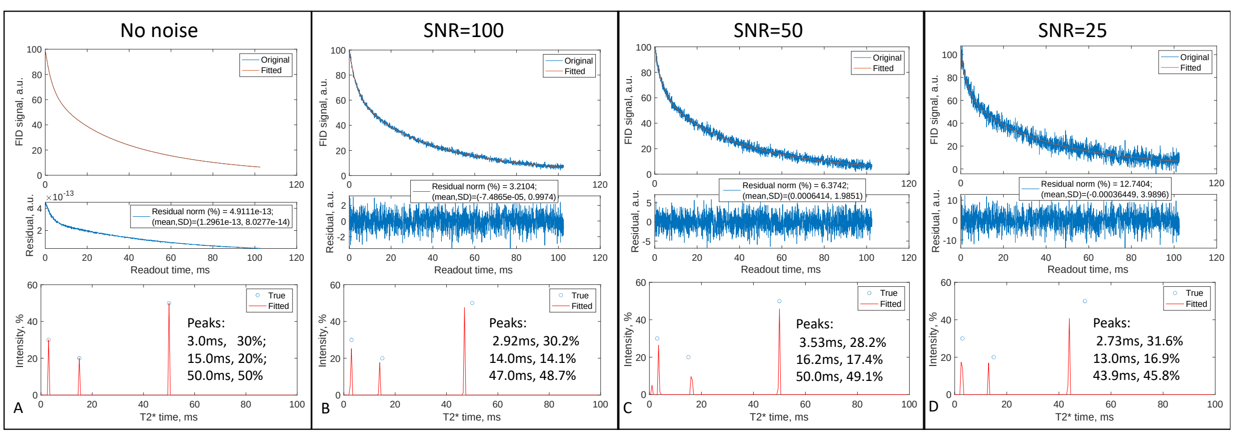

Fig. S3. Calculation stability of T_2* spectrum using the algorithm NNLS via MATLAB function *lsqnonneg(C,d)* and the numerical simulations at three popular components (circles o): $T_2*=(3, 15, 50)$ms with relative amplitudes A=(30, 20, 50) plus an additive random noise generated by function *randn(n,1)*. **(A)** – **(D)** are the simulations at $\Delta T_2* = 0.5$ms with noise at three typical values SNR = 100, 50, and 25. The peak parameters at doublets (bottom) were linearly combined with amplitude-weighting defined in equation S7. The best spectrum was achieved at SNR=100 among the three noisy cases.

Measurement stability of FID signals on whole brain: B_0 shimming

The B_0 shimming may change from subject to subject in routine practice, leading to a concern on the measurement stability of FID signals, thus the T_2* spectra, from whole brain across subjects. This concern is addressable because sodium (^{23}Na) MRI has about 4-fold lower resonance frequency than proton (^{1}H) MRI (e.g., 33.8 vs. 127.7 MHz at 3T), and the manual shimming (three iterations) is better than auto shimming. Fig. S4 shows the results of all the 15 subjects studied, with a small standard deviation (SD) in whole-brain histograms. There was no significant difference between the healthy and patient groups (P=0.908). Thus, the manual shimming, or ΔB_0, is stable.

Fig. S4. Measurement stability of FID signals on whole brain: B_0 shimming

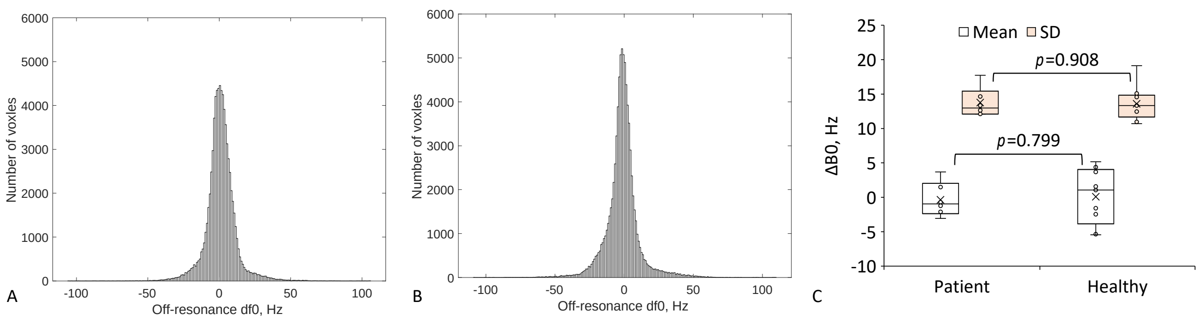

Fig. S4. Whole brain histograms of ΔB_0 mapping at TE_1/TE_2= 0.5/5ms under a manual shimming procedure (3 iterations). **(A)** A representative histogram from a healthy subject (52 years old, male), with mean±SD = 1.0±10.7 Hz. **(B)** A representative from a patient with epilepsy (31 years old, male), with mean±SD = -1.2±12.1 Hz. **(C)** Mean and SD distribution of whole brain ΔB_0 histograms from all the 15 study subjects (circles o) including 9 healthy and 6 patients, showing no significant difference between the two groups (healthy vs. patient), P = 0.799 for the mean and P = 0.908 for the SD.

Invisibility of CSF T_2 peaks in the spectrum: single T_2* mapping*

Cerebrospinal fluid (CSF) in the brain is known to have a T_2* value of ~50 ms as seen in single-T_2* maps (Figs. 7, 8). But this sodium population was not observed in the T_2* spectra. This phenomenon might be caused by small volume of CSF relative to whole brain. To confirm this cause, Fig. S5 presents two representative whole-brain histograms of single-T_2* mapping, with very small numbers of voxels (invisible bins) for CSF at T_2* around 50ms.

Fig. S5. Invisibility of CSF T_2* peak in the spectrum: single T_2* mapping.

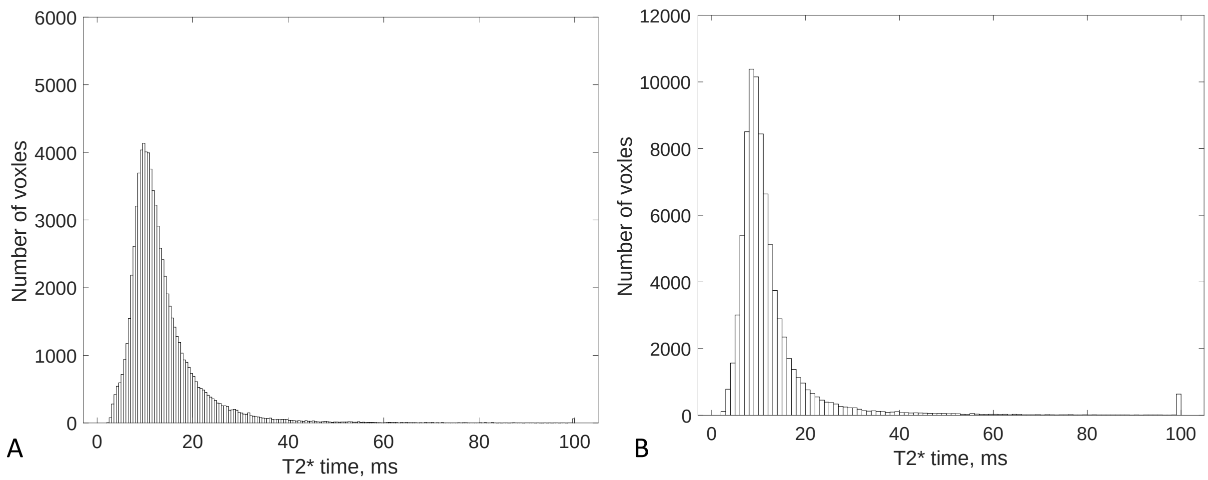

Fig. S5. Representative whole-brain histograms of single-T_2* mapping at TE_1/TE_2= 0.5/5ms. **(A)** A healthy subject (52 years old, male). **(B)** An epilepsy patient (31 years old, male). These, as well as the other healthy subjects and patients we studied, showed very small numbers (invisible bins) of voxels for CSF at T_2* ~ 50ms. Note: a visible bin at T_2*=100ms counts for voxels of T_2* values >= 100ms.